Intermittent flow regimes near the convection threshold in ferromagnetic nanofluids

Marina T. Krauzina, Alexandra A. Bozhko,* and Gennady F. Putin
Department of Physics, Perm State National Research University, 15 Bukirev Street, Perm 614990, Russia

Sergey A. Suslov
Department of Mathematics H38, Swinburne University of Technology, Hawthorn, Victoria 3122, Australia
(Received 4 September 2014; revised manuscript received 9 December 2014; published 20 January 2015)

The onset and decay of convection in a spherical cavity filled with ferromagnetic nanofluid and heated from below are investigated experimentally. It is found that, unlike in a single-component Newtonian fluid where stationary convection sets in as a result of supercritical bifurcation and where convection intensity increases continuously with the degree of supercriticality, convection in a multicomponent ferromagnetic nanofluid starts abruptly and has an oscillatory nature. The hysteresis is observed in the transition between conduction and convection states. In moderately supercritical regimes, the arising fluid motion observed at a fixed temperature difference intermittently transitions from quasiharmonic to essentially irregular oscillations that are followed by periods of a quasistationary convection. The observed oscillations are shown to result from the precession of the axis of a convection vortex in the equatorial plane. When the vertical temperature difference exceeds the convection onset value by a factor of 2.5, the initially oscillatory convection settles to a steady-state regime with no intermittent behavior detected afterward. The performed wavelet and Fourier analyses of thermocouple readings indicate the presence of various oscillatory modes with characteristic periods ranging from one hour to several days.

DOI: 10.1103/PhysRevE.91.013010 PACS number(s): 47.20.−k, 44.25.+f, 47.57.−s

I. INTRODUCTION

Ferromagnetic nanofluids are synthesized colloidal dispersions of single-domain solid magnetic (iron, cobalt, or magnetite) particles suspended in a carrier fluid, usually kerosene, mineral oil, or water. Such colloids respond strongly to an externally applied magnetic fields, which provides an opportunity for nonmechanical control of their flows. This feature defines a wide range of technological applications of ferromagnetic nanofluids, including thermal management systems in power transformers, solar batteries, microelectronics, and equipment operating in low gravity conditions [1–4]. Since the concentration of a solid phase in ferromagnetic nanofluids does not exceed 10%, it can be reasonably assumed that such nanofluids remain Newtonian; refer, for example, to experimental measurements reported in [5,6] and the discussion given in [7]. Yet the presence of solid particles leads to a qualitatively different flow regime in such fluids even in the absence of a magnetic field. This intricate fluid flow behavior that is not brought about by non-Newtonian effects and is not influenced by the application of a magnetic field is the subject of our current experimental study. We clarify from the outset that even though we will not consider fluid magnetization here, we will still refer to the working fluid as ferromagnetic nanofluid rather than just a nanofluid to emphasize its composition. We expect that the physical mechanisms causing flow behaviors similar to those we report here for ferromagnetic nanofluids may also act in other nanofluids containing nonmagnetic particles. However, we prefer not to overgeneralize our results until experimental data for nonferrous nanofluids become available.

To prevent solid particles from forming aggregates in the bulk of a fluid, they are covered with a surfactant such as oleic acid. Due to the very small size of such particles (around 10 nm), Brownian motion prevents sedimentation of the particles. Therefore, it is frequently assumed that the physical properties of such ferromagnetic nanofluids remain uniform and that the effects of a partial separation of nanofluids into fractions can be neglected, and it is common to consider ferrocolloids as hypothetical single-component fluids. Our experiments show that such a simplified treatment does not always produce accurate results. For example, computational results reported for a monocomponent model in [8,9] show that irregular regimes of convection arise only far beyond the convection threshold (i.e., for very large values of the governing flow parameters, such as thermal and magnetic Rayleigh numbers). The current experimental investigation of an actual ferromagnetic nanofluid demonstrates that this is not always so even in well-studied flow situations such as convection in a spherical cavity heated from below. Irregular convection regimes have been observed in the close vicinity of the thermogravitational convection threshold, and the characteristics of the arising flows have been found to depend on the history of the experiment.

The complex behavior of a ferromagnetic nanofluid is linked to a multitude of acting mechanisms of heat and mass transfer that are a consequence of a multicomponent composition of the fluid [10,11]. First, while adding surfactants drastically reduces the probability of the formation of solid particle aggregates, one cannot avoid them completely, and aggregates are prone to relatively quick gravitational sedimentation [12–14].

Secondly, the presence of solid particles in nonisothermal liquids leads to thermophoresis. The value of the (positive) Soret coefficient in ferromagnetic nanofluids is of the order of 10^{-1} K [15,16], which is an order of magnitude larger

*bozhko@psu.ru

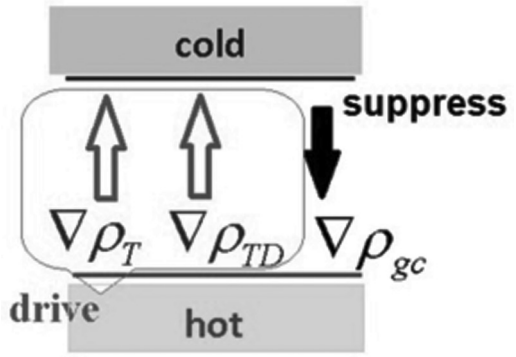

FIG. 1. Schematic diagram of the density gradients $\nabla\rho_T$, $\nabla\rho_{TD}$, and $\nabla\rho_{gC}$ caused by thermal expansion, thermal diffusion, and gravitational sedimentation, respectively, arising in a ferromagnetic nanofluid heated from below.

than the typical values reported for organic mixtures [17,18]. Therefore, a noticeable separation of species is expected to occur in ferromagnetic nanofluids if they are not actively mixed and remain nonuniformly heated for a sufficiently long time. This in turn influences the values of the overall fluid's transport coefficients [6,10,19].

Thirdly, while adding a surfactant reduces the fluid nonuniformity caused by solid particle aggregates, its presence (up to 10% of volume) can lead to thermodiffusion involving molecules of a surfactant and a carrier fluid. Moreover, the surfactant itself frequently contains multiple chemical components (e.g., oleic and linoleic acids) that are also subject to thermodiffusion [20]. Thermodiffusion can also be caused by the presence of molecules of different sizes and masses in the organic carrier fluid (kerosene, oil) [18].

All these compositional nonuniformities can result in a variation of the fluid density in a flow domain that may be hard to control yet could cause convective motion in a gravitational field. The qualitative diagram showing the main mechanisms

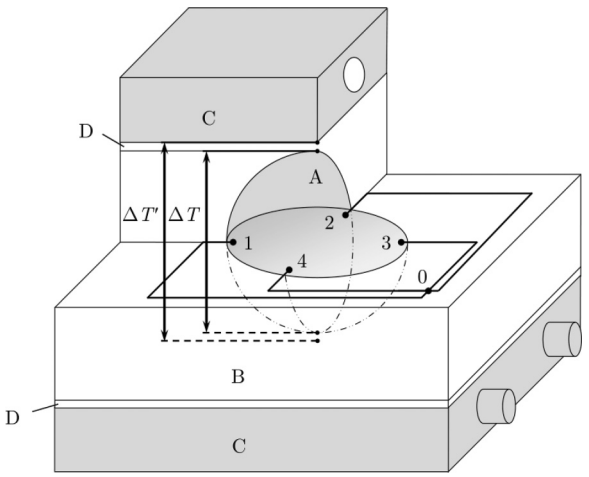

FIG. 2. Schematic of the experimental chamber: A—spherical cavity filled with a ferromagnetic nanofluid, B—Plexiglas plates, C—aluminum heat exchangers, D—Plexiglas inserts, 1, 2, 3, 4—thermocouples; ΔT and $\Delta T'$ are the temperature differences between the poles of the sphere and the heat exchangers, respectively.

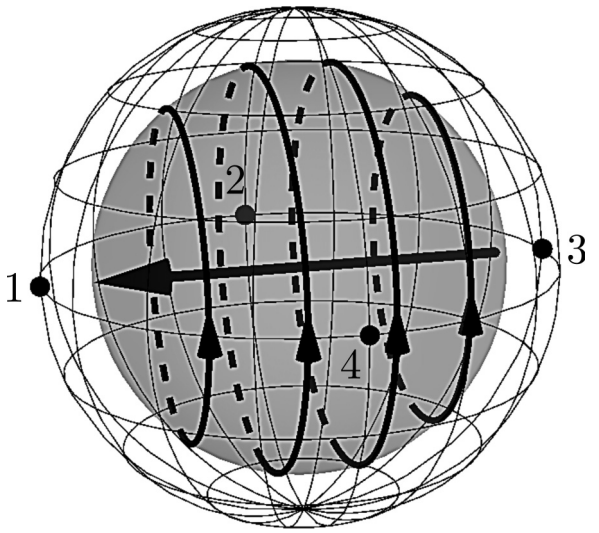

FIG. 3. Schematic view of a base vortex: 1, 2, 3, and 4 are thermocouples located in the equatorial plane (see Fig. 2); the arrow represents a vector of angular velocity of the first base convection vortex.

of heat and mass transfer in ferromagnetic nanofluids is shown in Fig. 1.

Thermal expansion of the fluid heated from below that causes the upward density gradient is the main destabilization mechanism of a static mechanical equilibrium in the system. Given that the Soret coefficient in ferronanofluids is positive (at least when no magnetic field is applied) [15,16], the heavy solid particles are drawn toward a cold wall. Thus thermodiffusion promotes the onset of convection in the fluid. In contrast, gravitational sedimentation of a solid phase delays the onset of convection. These convection mechanisms, albeit

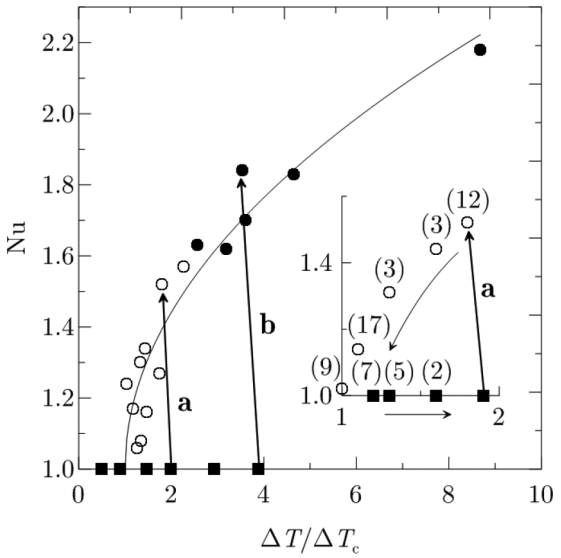

FIG. 4. The dependence of the Nusselt number (1) on the relative temperature difference $\Delta T/\Delta T_c$. The solid curve shows the least-squares fit to experimental data given by $\mathrm{Nu} = 1 + 0.44\sqrt{\Delta T/\Delta T_c - 1}$. The symbols are defined in the text. The experimental error bars are not shown to improve the readability of the figure.

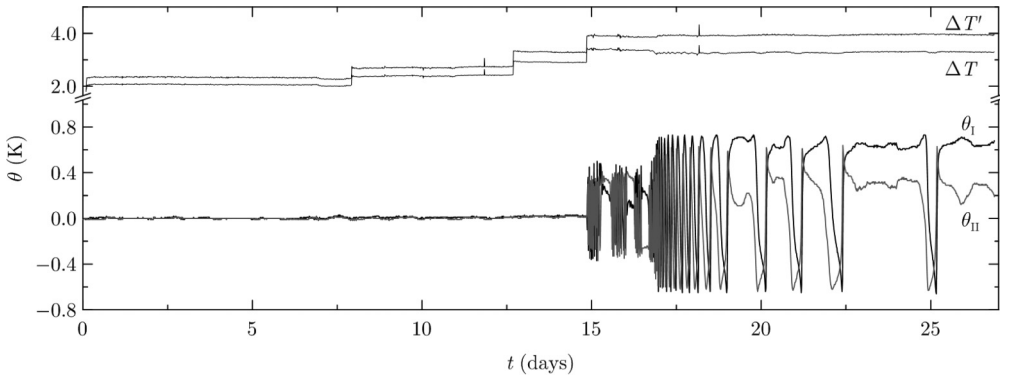

FIG. 5. The temperature time series for a sequence of stepwise increments of the temperature difference between the poles of a sphere. Convection was first detected once the relative temperature difference of $\Delta T = 1.9\Delta T_c$ was applied.

more diverse, are similar to those acting in doubly diffusive systems [21–25]. In addition, in cavities such as a sphere, diffusion-driven motion can arise in the proximity of solid surfaces that are inclined with respect to the mean fluid density gradient (see, e.g., Ref. [26]).

An additional difficulty in studies of ferromagnetic nanofluids arises due to the presence of rotational viscosity [27], which depends not only on the size and shape of nanoparticles and their aggregates but also on the type of local velocity profile and shear rate [6,10]. Unfortunately, measurements of rotational viscosity in dedicated experiments do not always provide the data that can be used for quantifying convection flows, as the flow conditions in viscosimeters are frequently very different from those in convection systems. In particular, the typical shear rates in convection flows are very small ($\sim 10^{-1}$ s^{-1}) compared to those achieved in viscosimeters ($\sim 10^{1}$–10^{2} s^{-1}) [6].

One of the main aspects that should be kept in mind when investigating convection flows of complex fluids is that the degree of species separation that leads to the density gradients capable of inducing flows is very small [10,28]. It can be estimated using a model problem of an isothermal horizontal layer of a colloid. If different constant concentrations of a heavy component are assumed at its top and bottom boundaries, the problem becomes analogous to the thermal Rayleigh-Bénard problem in a single-component fluid [28]. Species diffusion plays the role of thermal conduction, while the density gradient arises due to the variation of the concentration of the solid phase across the layer. If the direction of such a gradient is opposite to that of the gravity and its magnitude exceeds the critical value, the static mechanical equilibrium is destabilized and solutal convection starts. The control parameter defining the threshold in this case is the concentrational Rayleigh number $\mathrm{Ra}_C = \frac{\rho\beta_c g \Delta C d^3}{\eta D}$, where ρ is the fluid density, $\beta_c = \frac{1}{\rho}\frac{\partial \rho}{\partial C}|_T$ is the solutal expansion coefficient, g is the gravity, ΔC is the difference of the mass concentration of a solid phase, d is the thickness of a layer, η is the dynamic viscosity of the fluid, and D is the diffusion coefficient of solid particles. The well-known critical value of thermal Rayleigh number is $\mathrm{Ra} = \frac{\rho\beta g \Delta T d^3}{\eta\kappa} = 1708$, where $\beta = \frac{1}{\rho}\frac{\partial \rho}{\partial T}|_C$ is the coefficient of thermal expansion, ΔT is the temperature difference, and κ is the coefficient of thermal diffusivity. The manufacturer-specified properties of the transformer-oil-based ferromagnetic nanofluid [29] containing magnetite nanoparticles that was used in the current experiments were as follows: $\rho = 1.37 \times 10^3$ kg/m^3, $\eta = 0.069$ Pa s, $\kappa = 7.2 \times 10^{-8}$ m^2/s. The coefficients $\beta_C \approx 3$ and $D \approx 6 \times 10^{-13}$ m^2/s were estimated in separate experiments. Then for the layer of thickness $d \sim 1$ cm, upon setting $\mathrm{Ra}_C = \mathrm{Ra}$ we obtain the estimate for the onset of concentrational convection, $\Delta C \sim 10^{-8}$. Since magnetic fluids are opaque, optical refraction-based methods that are typically used to measure small concentration variations in transparent media are not applicable, thus it is practically impossible to measure such a small concentration difference directly. Yet such a weak concentrational nonuniformity results

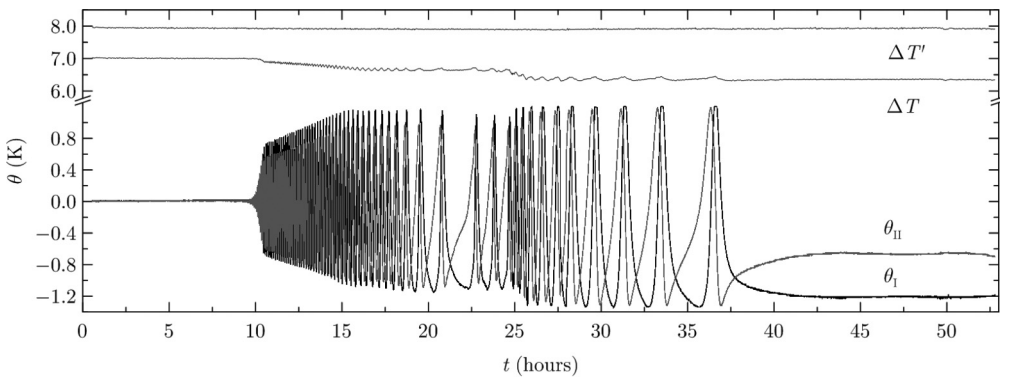

FIG. 6. The temperature time series illustrating the onset of oscillatory convection at $\Delta T = 3.9\Delta T_c$.

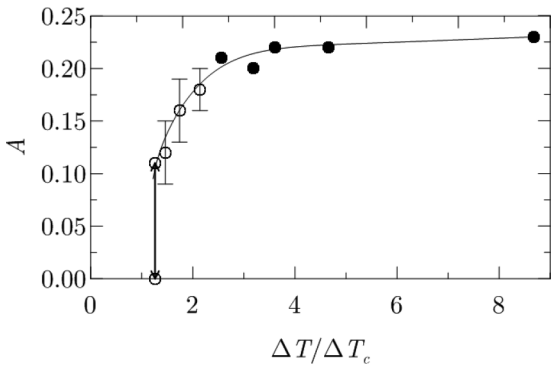

FIG. 7. The nondimensional amplitude of the signal recorded by the equatorial thermocouples as a function of the relative temperature difference. Solid and empty circles correspond to stationary and oscillatory regimes of convection in a premixed fluid, respectively. Vertical bars show the amplitude ranges detected for oscillatory convection.

in a macroscopic convection flow that can be detected using standard experimental techniques.

The complexity of the composition of ferromagnetic nanofluids and the multitude of heat and mass transfer mechanisms acting in them make their theoretical and numerical modeling an extremely challenging task. To date, most studies of that sort took into account only some of the mechanisms while neglecting the others. Thus the main goal of the current work has been to experimentally investigate the overall dynamics of a realistic ferromagnetic nanofluid subjected to the cumulative action of all physical driving mechanisms. This has been shown to lead to flow scenarios that differ qualitatively from those observed in single-component fluids and that have not yet been described theoretically or obtained numerically.

The paper is organized as follows. A description of the experimental setup and measurement method are given in Sec. II. The experimental results are reported in Sec. III. Discussion and concluding remarks are found in Sec. IV.

II. EXPERIMENTAL SETUP AND MEASUREMENT TECHNIQUE

The experimental setup is shown schematically in Fig. 2. A spherical cavity A of diameter $d = 16.0 \pm 0.1$ mm was cut in a Plexiglas [thermal conductivity $\lambda_P = 0.18$ W/(m K)] block B. The block consisted of two identical plates, each with the dimensions $53 \times 53 \times 8.0$ mm^3. To enable us to detect the onset of convection by measuring the change in heat transfer through the polar regions of the cavity using the Schmidt-Milverton method [30,31], two 1-mm-thick Plexiglas inserts D were attached to the block as shown in Fig. 2. This assembly was then placed between two aluminum heat exchangers C that were maintained at different constant temperatures by water pumped through them. The water temperature was controlled by jet thermostats KRIO-VT-01 [32] with an accuracy of 0.02 K. The cavity was filled with a nanofluid described in the previous section.

Differential copper-constantan thermocouples were used to register the temperature differences ΔT and $\Delta T'$ between the poles and the heat exchangers, respectively. Thermocouple wires were 0.1 mm in diameter. The calibrated thermocouple output was 40 μV K^{-1}. The thermocouple readings were recorded every $\Delta t_s = 5$ s (which is up to two orders of magnitude smaller than the characteristic flow development time) using the data acquisition system "THERMODAT" [33] and saved in text, database, and graphical formats using the in-house software package "THERMONET." The resolution of the system was 0.02 K, which corresponded to the relative error not exceeding 0.5%. The temperature drop $\Delta T_s = \Delta T' - \Delta T$ across the inserts that is proportional to the heat flux through the plate was then computed and plotted as a function of the temperature differences ΔT between the poles. The convection threshold was defined as the steady value of ΔT (observed for at least an hour) starting from which the ratio $\Delta T_s/\Delta T$ changed. The rationale for such an approach is briefly discussed below.

In the absence of convection, the steady temperature in a sphere heated from below is close to constant in any horizontal plane and varies approximately linearly in a vertical direction. In this case, the expression for the heat flux balance is $k\Delta T_s = \Delta T$, where k is an empirical constant characterizing the ratio of the effective heat conductivities of the Plexiglas and the fluid. The ratio

$$\mathrm{Nu} = k\frac{\Delta T_s}{\Delta T} = k\left(\frac{\Delta T'}{\Delta T} - 1\right) \tag{1}$$

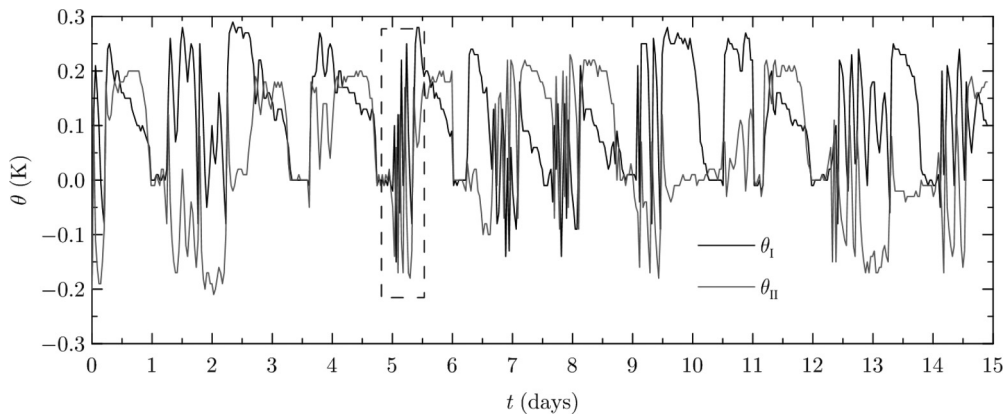

FIG. 8. The temporal evolution of the temperature response at $\Delta T = 1.2\Delta T_c$.

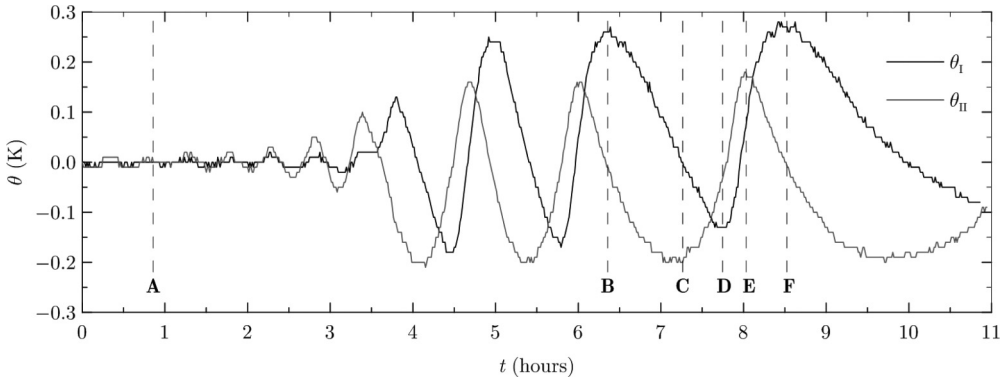

FIG. 9. The closeup of a region shown by a dashed frame in Fig. 8.

is known as the Nusselt number, and by definition it is unity for conduction regimes. However, when convection sets in the heat flux through the cavity increases and so does the value of the Nusselt number, which is the ratio of a full heat flux including convection and conduction components to the value of a conduction heat flux. It is clear then from the above definition of the Nusselt number that after convection starts, the ratio $\Delta T_s/\Delta T$ (or, equivalently, $\Delta T'/\Delta T$) has to increase.

To detect the structure of convective flows in a sphere, four additional thermocouples were placed equidistantly in the equatorial plane of the cavity, as shown in Fig. 2. Each thermocouple protruded 3 mm from the wall toward the center of a sphere and had a 1 mm soldered joint. The first flow instability mode in a sphere heated from below corresponds to a single convection vortex with an arbitrarily oriented horizontal axis parallel to the angular velocity vector $\boldsymbol{\omega}$ [28,31]. Such a motion can be considered as a superposition of two base vortices with the orthogonal axes containing the pairs of thermocouples 1 and 3 (see Fig. 3) and 2 and 4 (not shown). The vortices are characterized by the angular velocity vectors $\boldsymbol{\omega}_{\rm I}$ and $\boldsymbol{\omega}_{\rm II}$ such that $|\boldsymbol{\omega}|^2 = |\boldsymbol{\omega}_{\rm I}|^2 + |\boldsymbol{\omega}_{\rm II}|^2$. These vortices break the planar symmetry of the temperature distribution within a spherical cavity. For example, vortex $\boldsymbol{\omega}_{\rm I}$ leads to the appearance of the temperature difference detected in the equatorial plane by the diametrically opposite thermocouples 2 and 4; see Fig. 3. In the case of a nearly linear vertical temperature profile in the central part of the sphere, the magnitude $|\boldsymbol{\omega}|$ of the angular velocity is approximately proportional to the total convective perturbation $\theta = \sqrt{\theta_{\rm I}^2 + \theta_{\rm II}^2}$, where the component thermal perturbations are $\theta_{\rm I} = \theta_1 - \theta_3$ and $\theta_{\rm II} = \theta_2 - \theta_4$, and θ_1, θ_2, θ_3, and θ_4 are the readings of the corresponding thermocouples relative to their common juncture. Such thermocouple signals were used to establish the existence of various convective motions that have components in the form of vortices with horizontal axes [28].

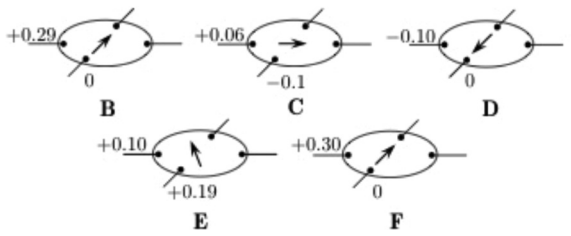

FIG. 10. The orientation of the vector of the angular velocity $\boldsymbol{\omega}$ of the convection vortex for time moments **B**–**F** in Fig. 9. The shown numerical values correspond to the thermocouple readings $\theta_{\rm I}$ and $\theta_{\rm II}$.

Finally, note that the flow phenomena observed in experiments occur on very different time scales: viscous diffusion time $t_v = d^2\rho/(\pi^2\eta)$, thermal diffusion time $t_t = d^2/(\pi^2 a)$, and particle diffusion time $t_D = d^2/(\pi^2 D)$. These are estimated as $t_v \sim 10^0$ s, $t_t \sim 10^2$ s, and $t_D \sim 10^7$ s. The shortest of these scales controlled the sampling interval and the longest determined the total duration of experiments.

III. RESULTS

The dependence of the Nusselt number on the relative temperature difference $\Delta T/\Delta T_{\rm c}$ between the poles of the sphere is shown in Fig. 4. Filled squares along the $\Delta T/\Delta T_{\rm c}$ axis correspond to regimes where the abrupt transition was detected. Empty circles correspond to self-induced oscillations that have been determined to be associated with the precession of the axis of the convection vortex in the equatorial plane. Filled circles depict the regimes of stationary single-vortex convection when the orientation of the flow axis did not change in time. The values of the Nusselt number are shown for oscillatory and stationary regimes that lasted from several days to several months at fixed thermal conditions.

As has been previously shown theoretically [28] and experimentally [31], a convective motion in a spherical cavity filled with a one-component Newtonian fluid heated from below arises in the form of a single stationary vortex as a result of a supercritical bifurcation when the applied temperature difference exceeds the critical value $\Delta T_{\rm c}$. A similar result has been established in the current experiments with a premixed multicomponent ferromagnetic nanofluid. To achieve good mixing, the experimental setup was turned sideways prior to the main observation run so that the heat exchanger plates became vertical. They were then maintained at the maximum possible temperature difference of 40 K for an hour. This induced a strong convective motion inside the sphere that ensured good mixing of the fluid. In experiments with such a homogeneous ferrocolloid, the convection threshold value of $\Delta T_{\rm c} = 1.8 \pm 0.1$ K was reproduced in several independent runs, and it has been used to construct Fig. 4.

In contrast, when preliminary mixing had not been performed, the convection was found to be established abruptly,

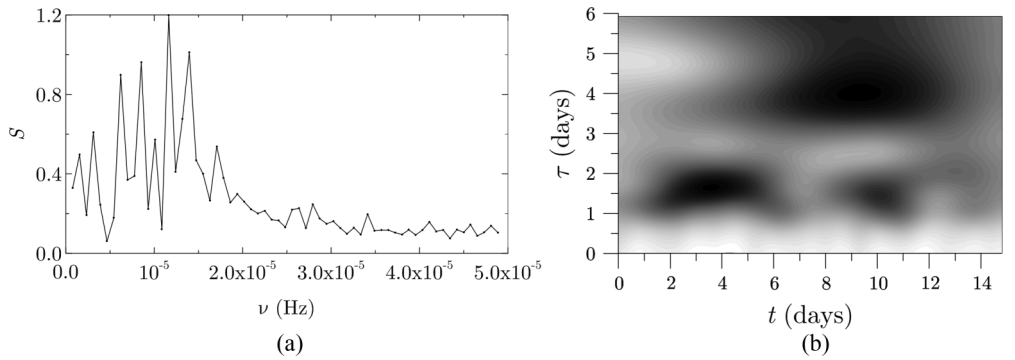

FIG. 11. (a) The spectral density S and (b) the magnitude of Morlet wavelet coefficients for the thermocouple signal θ_1 recorded for $\Delta T = 1.2\Delta T_c$. The darker shade corresponds to the larger value of the coefficient amplitude.

which is of major interest in the current study. Hysteresis was observed when a gradual increase of the applied temperature difference had been reversed. The arrows labeled "**a**" and "**b**" in Fig. 4 show the examples of such abrupt transitions from a static mechanical equilibrium to convection that were detected when the fluid remained static for about a month prior to the start of experiments [34]. The closeup shows the typical hysteresis when a sequence of the stepwise increments of the temperature difference between the poles of the sphere was followed by that of stepwise decreases. The figures in parentheses give the observation time (in days) in each thermal regime. The finite amplitude convection flow was abruptly induced at $\Delta T = 1.9\Delta T_c$; see arrow "**a**." The time series record shown in Fig. 5 provides details of this transition. The fluid remained isothermal and at rest for 25 days before the temperature difference $\Delta T = 1.2\Delta T_c$ was applied between the poles of the sphere. This regime was maintained for 7 days with no convection detected (see the first horizontal line segment in Fig. 5). Subsequently, the temperature difference was increased to $\Delta T = 1.3\Delta T_c$, which was observed for 5 days, and then to $\Delta T = 1.6\Delta T_c$ for 2 days. No convection was detected in these regimes either (see the second and third horizontal line segments in Fig. 5). However as soon as the applied temperature difference was set to $\Delta T = 1.9\Delta T_c$ (day 15 in Fig. 5), the finite amplitude oscillatory convection started.

A similar abrupt transition to a finite amplitude convection state (not shown) was observed when the temperature difference $\Delta T = 2.0\Delta T_c$ was applied to a sphere filled with an initially isothermal fluid that remained at rest for only 3 days. In this case, the convection vortex with the axis precessing in the equatorial plane appeared 29 h after the temperature difference was applied.

The thermogram corresponding to the transition shown by arrow "**b**" in Fig. 4 is given in Fig. 6. In this case, the fluid remained at rest in isothermal conditions for 34 days prior to the start of experiment. Then the temperature difference between heat exchangers was applied in a stepwise manner with four equal temperature increments of 2 K each. After each temperature difference increase, the system was left to adjust for 24 h. The convection starts the form of quasiharmonic oscillations 10 h after the temperature difference of 8 K between the heat exchangers was applied (the left edge of Fig. 6), which corresponded to $\Delta T = 3.9\Delta T_c$. Their period increased from 6 min during the first few hours after the onset to around 3 h a day later. Such oscillations were observed for 27 h before they gave way to a steady convection in the form of a single vortex with a fixed orientation of its axis in the equatorial plane. As seen from the thermal records presented in Fig. 6, the variation of the amplitude of oscillations detected by the equatorial thermocouples leads to the change of the temperature difference between the poles of the cavity, which in turn results in the variation (of the order of several percent) of the heat flux through the fluid; see Eq. (1).

In contrast, in the reverse transition, when the temperature difference between the poles is being reduced, the transition

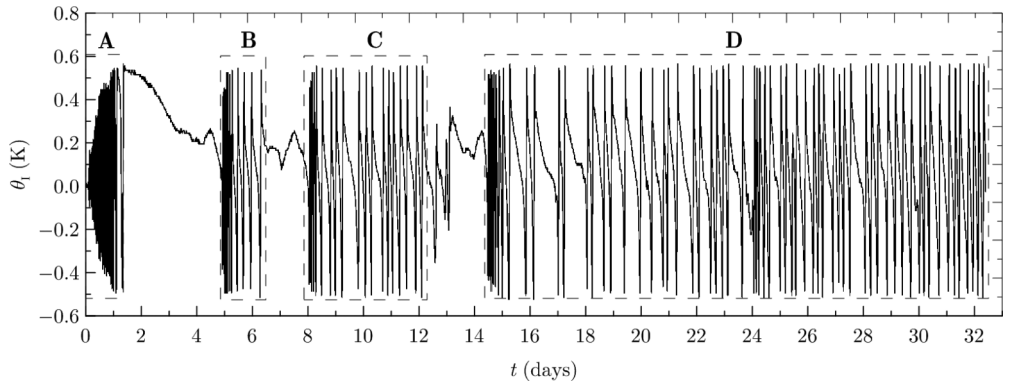

FIG. 12. The temporal evolution of the temperature response θ_1 at $\Delta T = 1.8\Delta T_c$.

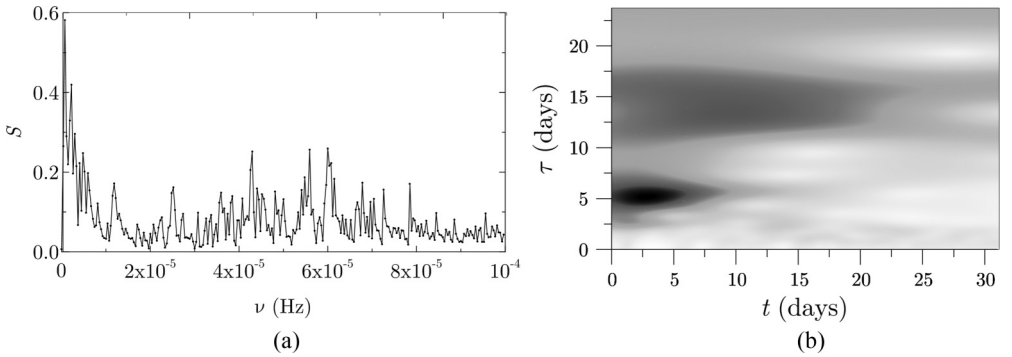

FIG. 13. Same as Fig. 11 but for $\Delta T = 1.8\Delta T_c$.

to a motionless state is characterized by a gradual decrease of the flow amplitude to zero at $\Delta T = \Delta T_c$; see the curve shown by the solid line in Fig. 4.

The experiments with a non-premixed ferromagnetic nanofluid indicate that the particle concentration gradient arising due to the gravitational sedimentation enhances the stability of a mechanical equilibrium in such a fluid. Even if a large destabilizing temperature gradient is applied to non-premixed fluid (see arrow "**b**" in Fig. 4), it takes a significant amount of time for convection to start. Such a delay is not observed in single-component fluids or well-mixed nanofluids. This indicates that the gravitational sedimentation of particles is counteracted by a thermodiffusion that gradually reduces the stabilizing density gradient and eventually leads to the onset of convection in the initially gravity-stratified ferromagnetic nanofluids.

It is convenient to illustrate the details of the convection onset using the nondimensional amplitude of a thermal signal defined as

$$A = \frac{\theta}{\Delta T}. \tag{2}$$

It remains zero for pure conduction states. When convection sets in, three regimes are clearly distinguished in a premixed fluid; see Fig. 7. For sufficiently large values of the applied temperature difference, the convection begins in the form of a stationary vortex with a fixed amplitude and orientation of the axis. At the moderately supercritical values of the temperature difference, the axis of convection vortex precesses in the equatorial plane and the vortex amplitude varies within the range shown by vertical bars in Fig. 7. Perhaps the most peculiar behavior is observed near the threshold of convection. In these regimes, convection has an intermittent character. It arises spontaneously and leads to a sharp increase of the amplitude from $A = 0$ (conduction regime) to $A \approx 0.11$ (convection regime); see the upward arrow in Fig. 7. Subsequently, such convection decays, as shown in the figure by the downward arrow. However, approximately 6 h later, convection arises again and the cycle repeats, as seen from Fig. 8 (nine cycles are shown). Therefore, in the vicinity of the convection threshold, intermittent regimes, in which oscillatory convection spontaneously arises and completely decays, are detected. The details of one such cycle are demonstrated in Fig. 9.

When both thermal readings θ_I and θ_{II} are zero (e.g., time **A** in Fig. 9), no convection exists in the cavity. When $\theta_I > 0$ (times **B** and **F**), the fluid rises at the location of thermocouple 1 (see Fig. 3) and sinks near thermocouple 3. The flow direction is reversed if $\theta_I < 0$ (time **D**). Similarly, the direction of the flow induced by the second component vortex is determined by monitoring the sign of θ_{II}: if $\theta_{II} > 0$, the fluid rises near thermocouple 2 and sinks near thermocouple 4 (time E) and vice versa (time **C**). The orientation of the vector of the angular velocity $\boldsymbol{\omega}$ of the convection vortex estimated from the thermocouple data for time moments **B**–**F** in Fig. 9 is shown in Fig. 10. This diagram demonstrates that the axis of the convection vortex rotates in the equatorial plane of the sphere.

Fourier and Morlet wavelet-based analyses have been applied to the signals registered by the equatorial thermocouples in order to determine their detailed spectral characteristics. For example, a Fourier spectral density distribution computed

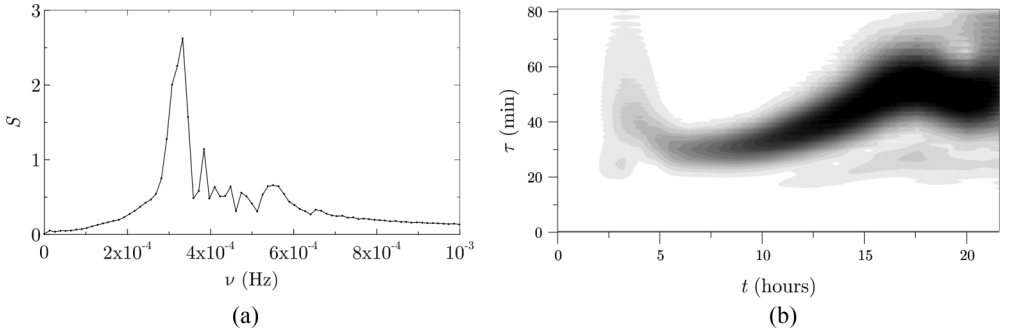

FIG. 14. (a) The spectral density S and (b) the magnitude of Morlet wavelet coefficients for the thermocouple signal θ_I recorded for $\Delta T = 1.8\Delta T_c$ for interval **A** (day 1) in Fig. 12. The darker shade corresponds to the larger value of the coefficient amplitude.

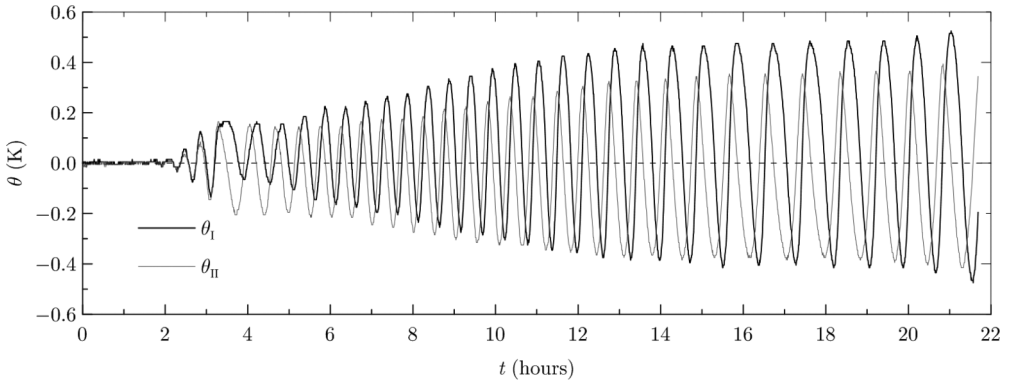

FIG. 15. Details of the temporal evolution of the temperature response θ_{I} and θ_{II} at $\Delta T = 1.8\Delta T_{\mathrm{c}}$ for interval **A** (day 1) in Fig. 12.

for a thermocouple signal θ_{I} recorded for $\Delta T = 1.2\Delta T_{\mathrm{c}}$ is shown in Fig. 11(a). It indicates the presence of the four main frequencies $\nu_{1,2,3,4} \approx (0.6, 0.8, 1.2, 1.4) \times 10^{-5}$ Hz corresponding to periods of 1.9, 1.4, 1.0, and 0.8 days, respectively.

The coefficients of the wavelet transform of a discrete time series θ_k sampled at times $t_k = k\Delta t_s$, $k = 1,2,\ldots,n$, where n is the total number of readings, have been computed as

$$W_{u,s} = \frac{1}{\sqrt{s}} \sum_{k=1}^{n} \theta_k \psi\left(\frac{k-u}{s}\right). \tag{3}$$

Here $\psi(\frac{k-u}{s})$ is the base wavelet of scale $s\Delta t_s$ evaluated at time $t_k = k\Delta t_s$ and shifted by $u\Delta t_s$ [35]. Each such wavelet represents a contribution to the overall signal that is observed at $t = (k-u)\Delta t_s$ and has a characteristic time span of $\tau = s\Delta t_s$. The magnitudes of the coefficients were computed using the wavelet analysis routines implemented in MATHEMATICA [36] for $u = 1,2,\ldots,n$ and the values of s ranging from 1 to $n/2$. The wavelet transform of a thermocouple signal θ_{I} recorded for $\Delta T = 1.2\Delta T_{\mathrm{c}}$ is shown in Fig. 11(b). The dark regions indicate the presence of temporal structures with the characteristic periods ranging from 1 to 2 days during days 2–5 and 9–11 and from 3.5 to 4.5 days during days 7–12 of the experiment.

Further away from the critical point (for $\Delta T > 1.2\Delta T_{\mathrm{c}}$), the qualitative behavior of the system changes. A typical record of a thermocouple signal is shown in Fig. 12. The regimes of slow variation over the time intervals lasting for 1–2 days when the axis of the convection vortex rotates by a small angle in the equatorial plane alternate with regimes of relatively fast precession of the vortex axis with the period ranging from tens of minutes to several hours. Such regimes are shown by empty circles in Figs. 4 and 7. The Fourier spectral density and the wavelet transform coefficients of the corresponding thermal signal are presented in Fig. 13. The main maximum of the Fourier spectral density curve in Fig. 13(a) corresponds to $\nu \approx 0.7 \times 10^{-6}$ Hz (the period of 16.5 days). It is seen from the Morlet wavelet transform [Fig. 13(b)] that the overall signal initially contained dominant oscillations with a period of approximately 5 days that have been replaced with the slower oscillations with periods in the range between 12 and 17 days in later observations.

The thermogram presented in Fig. 12 indicates that four oscillatory bursts labeled **A** (day 1), **B** (days 5–7), **C** (days 8–12), and **D** (days 15–35) separated by the intervals of a slow rotation of the axis of a convection vortex were observed for the applied temperature difference $\Delta T = 1.8\Delta T_{\mathrm{c}}$. They are discussed in detail next.

During the first day after the start of the experiment, the oscillatory convection is established. The wavelet coefficients and spectral density plots of the time series corresponding to interval **A** in Fig. 12 and shown in Fig. 14 indicate that the dominant frequency of a signal during this time is $\nu \approx 3.3 \times 10^{-4}$ Hz, which corresponds to the period of about 50.5 min.

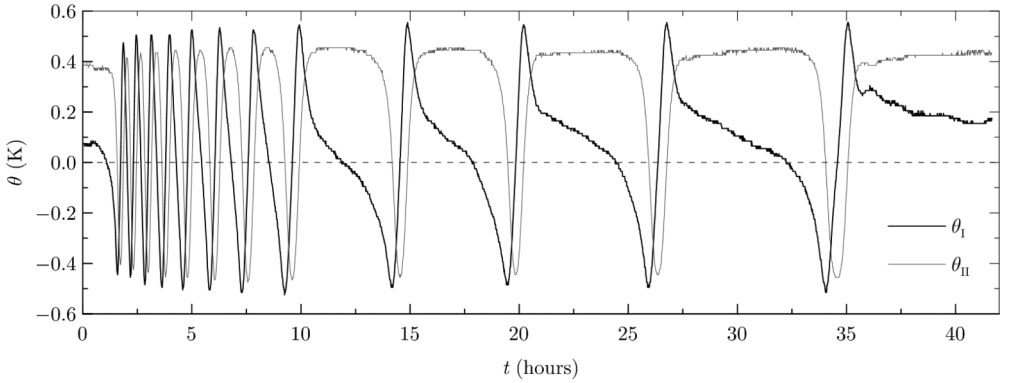

FIG. 16. Same as Fig. 15 but for interval **B** (days 5–7) in Fig. 12.

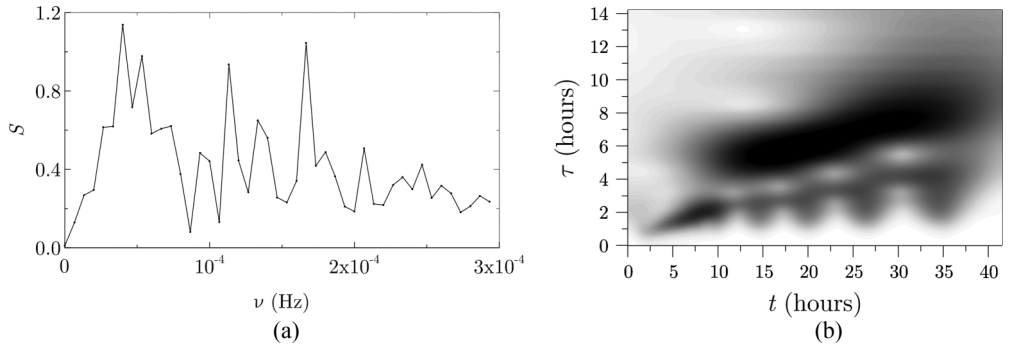

FIG. 17. Same as Fig. 14 but for interval **B** (days 5–7) in Fig. 12.

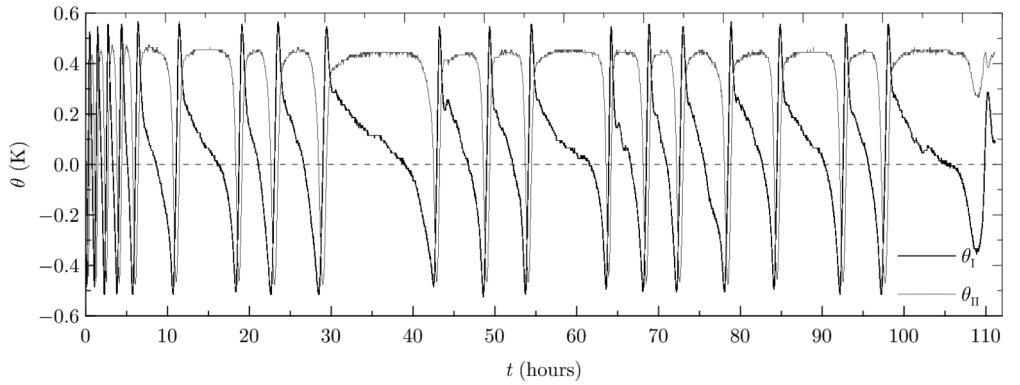

FIG. 18. Same as Fig. 15 but for interval **C** (days 8–12) in Fig. 12.

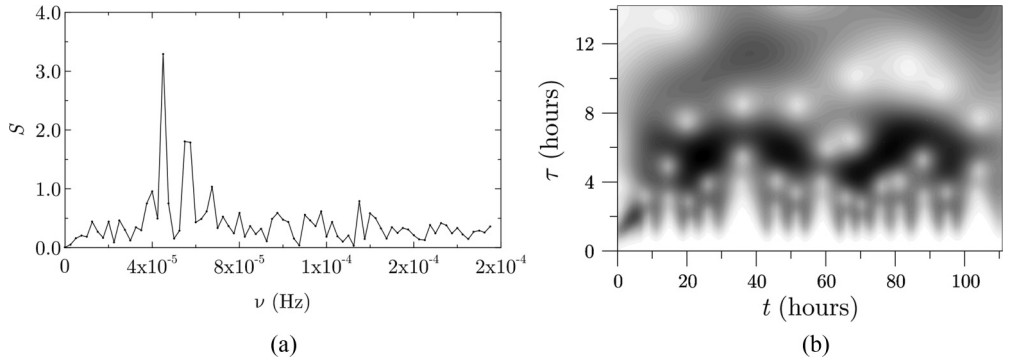

FIG. 19. Same as Fig. 14 but for interval **C** (days 8–12) in Fig. 12.

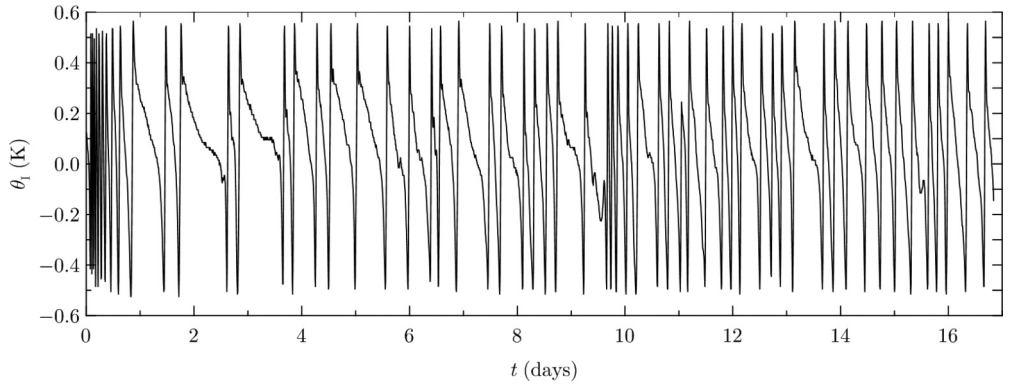

FIG. 20. Same as Fig. 15 (only θ_{I} is shown) but for interval **D** (days 15–35) in Fig. 12.

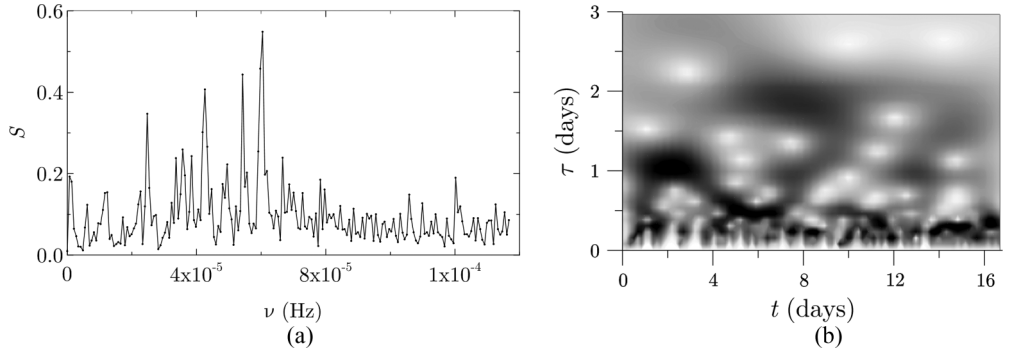

FIG. 21. Same as Fig. 14 but for interval **D** (days 15–35) in Fig. 12.

The amplitude of the oscillatory component of a convection flow initially increases approximately linearly with time until it saturates after about 13 h. The plot of Morlet wavelet transform coefficients in Fig. 14(b) shows that from this point the period of oscillations starts slowly increasing, which is indeed seen in Fig. 15.

For the second oscillatory burst **B**, shown in detail in Fig. 16, the spectral density presented in Fig. 17(a) indicates the presence of four dominant frequencies $\nu_{1,2,3,4} \approx (0.4, 0.5, 1.1, 1.7) \times 10^{-4}$ Hz corresponding to oscillations with periods 6.9, 5.2, 2.5, and 1.7 h, respectively. However, as follows from the wavelet analysis summarized in Fig. 17(b), these periods do not correspond to four distinct harmonic modes but rather represent two oscillatory modes whose periods increase monotonically in time from approximately 1 to 4 and from 5 to 8 h over the intervals of 2–37 and 10–35 h, respectively.

The third oscillatory burst shown in Fig. 18 is characterized by two dominant oscillatory components corresponding to two frequencies $\nu \approx 0.45 \times 10^{-4}$ and 0.56 Hz corresponding to periods of 6.1 and 5 h, respectively [see Fig. 19(a)]. However, the wavelet transform presented in Fig. 19(b) shows a qualitative difference in the signal behavior during interval **C**: in contrast to the regimes observed at earlier times, the period of oscillations does not increase monotonically with time but rather it increases and decreases periodically around their average values (oscillation periods vary between 4 and 7 h).

The main feature of oscillatory convection observed during interval **D** (see Figs. 12 and 20) is that the flow becomes less regular: the spectral density peaks shown in Fig. 21(a) are less pronounced and the spectrum widens in comparison to that shown for intervals **A**–**C**. As evidenced by Fig. 21(b), the oscillation periods tend to decrease from about 1 day in the beginning of the burst to less than 0.5 days by the end of the recorded experiment.

Thus when a moderately supercritical temperature difference is applied, the convection begins in the form of oscillations that are nearly harmonic in the beginning of the experiment and become progressively irregular as time progresses. The regimes of well-defined oscillations initially alternate with those of nearly stationary convection. The duration of the latter decreases with time, and eventually irregular unsteady convection sets in after a number of discrete oscillatory bursts.

IV. DISCUSSION AND CONCLUSIONS

The likely explanation for the peculiar behavior of a ferromagnetic nanofluid heated from below described in Sec. III is that when the temperature gradient applied to the resting ferromagnetic nanofluid remains small, the nanoparticles of heavy solid phase drift preferentially in the direction of gravity. Therefore, a stabilizing density gradient is established over time. It is commonly assumed that because of the small size of solid particles, such a sedimentation would occur on a very long time scale and therefore its effects can be neglected at least in short-time experiments. This simplified approach may be acceptable in some applications, but our parametric estimates and experiments show that convection flows are extremely sensitive to and are easily modified by very small fluid nonuniformities such as the vertical density gradient caused by sedimentation. In particular, because of its presence, convection in a ferromagnetic nanofluid first occurs abruptly and at a larger temperature difference than it would in a hypothetical uniform single-component fluid with transport properties given in Sec. I. Yet the reverse transition from convection to a static conduction state is observed at the smaller values of the governing parameters, which agree well with the critical values for single-component fluids [31]. Such an observation is consistent with the hypothesis of the gravitational separation of species in a ferromagnetic nanofluid: once convection sets in, it mixes the fluid removing the sedimentation effects. Therefore, the behavior of a ferromagnetic nanofluid becomes similar to that of a single-component Newtonian fluid. Since the reverse transition to static equilibrium from a convection state is naturally initiated from a well-mixed state, it occurs smoothly and convection persists up to a lower value of the temperature gradient that is now defined, similarly to monofluids, only by the balance between the thermal expansion of the fluid and its viscosity.

The effect of sedimentation also offers a plausible explanation of the decay of convection in long-term observations near the threshold where the flow amplitude is relatively small. In this case, despite the existence of weak mixing, its intensity is not sufficiently high to overcome the sedimentation effects completely. Thus a stabilizing density gradient is established over time that leads to the decay of convection. The sedimentation effect, however, cannot explain the spontaneous rebirth of convection observed in intermittent regimes near the threshold. Thus we are led to conclude that yet another physical

mechanism influences the flow of ferromagnetic nanofluids. It is likely that thermodiffusion driving heavy solid particles upward toward the cool regions counterbalances the effect of sedimentation and leads to the reemergence of convection.

Another noteworthy observation made in our experiments is the precession of the axis of a convection vortex in the equatorial plane of the cavity. A similar effect was reported previously in long-term observations of a drift of convection cells in planar Bénard-Marangoni convection reported in [37,38]. There, the hypothesis was put forward that such a drift could be caused by the Coriolis force due to the Earth's rotation. However, geometrical considerations of the current spherical geometry show that the Coriolis force could at most lead to the north-south alignment of the axis of a convection vortex, but not to its continuous rotation as illustrated in Fig. 10. It is also of interest to note that previous experiments on convection in a water-filled sphere did not reveal any oscillatory regimes [31]. Therefore, it is likely that the physical reason for the precession is linked to a complex composition of ferromagnetic nanofluids, however the exact mechanism of this phenomenon remains unclear.

To summarize, our experiments demonstrated that convection in a spherical cavity filled with ferromagnetic nanofluid heated from below leads to three qualitatively different types of motion. In the vicinity of the convection threshold, the convection regime is intermittent: low-frequency oscillations caused by the precession of the axis of the convection vortex in the equatorial plane decay periodically so that the system returns to rest prior to entering another oscillatory state. At moderate supercritical temperature differences, the system repeatedly transits from high- to low-frequency oscillation states that are followed by relatively short periods of slow nonoscillatory variations of convection flow amplitude and orientation. In strongly supercritical regimes, abrupt transitions between nearly stationary convection states characterized by different flow amplitudes and orientations are detected. Such rich behavior in a system with simple geometry is attributed to the intricate interplay between thermal expansion, diffusion, and sedimentation effects that arise due to the compositional complexity of ferromagnetic nanofluids that are currently used in various industrial and scientific applications. The flow regimes detected experimentally in this work have not been reported in previous analytical, numerical, or experimental studies of single-component fluids. Therefore, the widely used model treatment of ferromagnetic nanofluids as well-mixed hypothetical monofluids may not be adequate when applications of interest operate in intermittent or slow flow regimes.

We also note that throughout our presentation, we emphasized the composition of the experimental fluid by referring to it as ferromagnetic nanofluid even though no magnetic control that ferrofluids are purposefully designed for has been applied. It may be tempting in this situation to view the used working fluid just as a generic nanofluid, i.e., as a suspension of solid nanoparticles in a carrier fluid. However, we intentionally avoided such a generalization since it may be possible that the flows of nanofluids containing different chemical components could differ from those reported here. For example, this could be due to the dependence of the sign of a thermodiffusion coefficient on the fluid composition (for surfacted ferromagnetic nanofluid similar to those used in our experiments, it remains positive (see, e.g., Ref. [15]), but this does not have to be the case for all nanocolloids). Thus experiments similar to those reported here but conducted with different nanofluids are required to shed further light on and quantify flows of various nanofluids. The most serious obstacle in the way of such experiments is the time needed to conduct them (e.g., experiments reported here for a single type of nanofluid required more than two years to complete). Thus while the drastic distinction of nanofluid flows from those of single-component fluids that we have detected in the reported experiments warrants further investigation, it appears that the only way conclusive and comprehensive knowledge of the behavior of nonisothermal nanofluids can be generated is via the effort distributed among several research groups.

ACKNOWLEDGMENTS

The work was partially supported by Grant No. NSh-4022.2014.1 from the Grant Council of the President of the Russian Federation as part of the National Program for Supporting Leading Scientific Schools.

[1] Y. Cao, X.-R. Zhang, and H. Yamaguchi, Experimental study on convective heat transfer of nanofuids in solar energy system, in *The Abstract Book of the Twelfth International Confedrence on Magnetic Fluids* (Tohoku University, Sendai, Japan, 2010), pp. 135–136.

[2] W. Lian, Y. Xuan, and Q. Li, Design method of automatic energy transport devices based on the thermomagnetic effect of magnetic fluids, Int. J. Heat Mass Transfer **52**, 5451 (2009).

[3] S. Odenbach, Microgravity experiments on thermomagnetic convection in magnetic fluids, J. Magn. Magn. Mater. **149**, 155 (1995).

[4] S. Odenbach, *Ferrofluids: Magnetically Controllable Fluids and their Applications* (Springer, New York, 2002).

[5] G. P. Bogatyrev and V. G. Gilev, Concentration dependence of the viscosity of a magnetic liquid in an external field, Magnetohydrodynamics **20**, 249 (1984).

[6] S. Odenbach, *Magnetoviscous Effects in Ferrofluids* (Springer, New York, 2002).

[7] H. Rahman and S. A. Suslov, Thermomagnetic convection in a layer of ferrofluid placed in a uniform oblique external magnetic field, J. Fluid Mech. **764**, 316 (2015).

[8] I. Kobori and H. Yamaguchi, Thermomechanical instability and chaotic state, J. Magn. Magn. Mater. **122**, 290 (1993).

[9] D. Laroze, P. G. Siddheshwar, and H. Pleiner, Chaotic convection in a ferrofluid, Commun. Nonlinear Sci. **18**, 2436 (2013).

[10] E. Blums, A. O. Cebers, and M. M. Maiorov, *Magnetic Fluids* (Walter de Gruyter, Berlin, 1997).

[11] V. I. Terekhov, S. V. Kalinin, and V. V. Lehmanov, The mechanism of heat transfer in nanofluids: State of the art (review). Part 2. Convective heat transfer, Thermophys. Aeromechan. **17**, 157 (2010).

[12] A. F. Glukhov and G. F. Putin, Attainment of the equilibrium barometric distribution of magnetic fluid particles, in *Hydrodynamics: Collection of Papers (in Russian)*, edited by D. V. Lyubimov, Vol. 12 (Perm State University, Perm, Russia), pp. 92–103.

[13] E. V. Lakhtina, Centrifugation of dilute ferrofluids, Phys. Proc. **9**, 221 (2010).

[14] A. F. Pshenichnikov, E. A. Elfimova, and A. O. Ivanov, Magnetophoresis, sedimentation, and diffusion of particles in concentrated magnetic fluids, J. Chem. Phys. **134**, 184508 (2011).

[15] G. Demouchy, A. Mezulis, A. Bee, D. Talbot, J. C. Bacri, and A. Bourdon, Diffusion and thermodiffusion studies in ferrofluids with a new two-dimensional forced Rayleigh-scattering technique, J. Phys. D **37**, 1417 (2004).

[16] T. Völker, E. Blums, and S. Odenbach, Determination of the Soret coefficient of magnetic particles in a ferrofluid from the steady and unsteady part of the separation curve, Int. J. Heat Mass Transfer **47**, 4315 (2004).

[17] P. Kolodner, H. Williams, and C. Moe, Optical measurement of the Soret coefficient of ethanol/water solutions, J. Chem. Phys. **88**, 6512 (1988).

[18] J. K. Platten, The Soret effect: A review of recent experimental results, J. Appl. Mech. **73**, 5 (2006).

[19] A. O. Ivanov, S. S. Kantorovich, E. N. Reznikov, C. Holm, A. F. Pshenichnikov, A. Lebedev, A. Chremos, and P. J. Camp, Magnetic properties of polydisperse ferrofluids: A critical comparison between experiment, theory, and computer simulation, Phys. Rev. E **75**, 061405 (2007).

[20] A. F. Pshenichnikov (private communication).

[21] G. Ahlers, K. Lerman, and D. S. Cannell, Different convection dynamics in mixtures with the same separation ratio, Phys. Rev. E **53**, R2041(R) (1996).

[22] G. Donzelli, R. Cerbino, and A. Vailati, Bistable heat transfer in a nanofluid, Phys. Rev. Lett. **102**, 104503 (2009).

[23] F. Winkel, S. Messlinger, W. Schöpf, I. Rehberg, M. Siebenbürger, and M. Ballauff, Thermal convection in a thermosensitive colloidal suspension, New J. Phys. **12**, 053003 (2010).

[24] L. Kh. Ingel and M. V. Kalashnik, Nontrivial features in the hydrodynamics of seawater and other stratified solutions, Physics-Uspekhi **55**, 356 (2012).

[25] C. Beaume, A. Bergeon, and E. Knobloch, Convectons and secondary snaking in three-dimensional natural doubly diffusive convection, Phys. Fluids **25**, 024105 (2013).

[26] M. A. Page, Combined diffusion-driven and convective flow in a tilted square container, Phys. Fluids **23**, 056602 (2011).

[27] A. Einstein, On the movement of small particles suspended in a stationary liquid demanded by the molecular kinetic theory of heat, Ann. Phys. (Leipzig) **17**, 549 (1905).

[28] G. Z. Gershuni and E. M. Zhukhovitsky, *Convective Stability of Incompressible Fluid* (Keter, Jerusalem, 1976).

[29] Manufactured in Scientific Laboratory of Practical Ferromagnetic Fluids, Ivanovo, Russia under Technical Conditions 229-001-02068195-2002 using a transformer oil with density $\rho_{\mathrm{TO}} = 8.79 \times 10^2$ kg/m^3, dynamic viscosity $\eta_{\mathrm{TO}} = 0.020$ Pa s, and thermal conductivity $\lambda_{\mathrm{TO}} = 0.11$ W/(m K) as a carrier fluid containing 10% by volume of magnetite particles with the average density $\rho_{\mathrm{M}} = 5.1 \times 10^3$ kg/m^3 and the average size of 10 nm stabilized with an oleic acid with density $\rho_{\mathrm{OA}} = 8.95 \times 10^2$ kg/m^3, dynamic viscosity $\eta_{\mathrm{OA}} = 0.027$ Pa s, and thermal conductivity $\lambda_{\mathrm{OA}} = 0.23$ W/(m K). The thermal conductivity of the ferromagnetic nanofluid was $\lambda_{\mathrm{FNF}} = 0.15$ W/(m K). All properties are listed for a temperature of 20 °C.

[30] R. J. Schmidt and S. W. Milverton, On the instability of a fluid when heated from below, Proc. R. Soc. London, Ser. A **152**, 586 (1935).

[31] A. P. Ovchinnikov and G. F. Shaidurov, Convective stability of homogeneous fluid in a spherical cavity, Hydrodynamics. Perm State University (in Russian) **1**, 3 (1968).

[32] TERMEX, Tomsk, Russia. KRIO-VT-01.

[33] Scientific and Industrial Organisation "Control Systems," Instrument Engineering Division, Ltd., Perm, Russia. TermoDat-38B1.

[34] The transition to convection leads to a slight decrease in the temperature difference ΔT between the poles of the sphere (see a slight leftward inclination of the arrows showing the transition in Fig. 4) even though the temperature difference $\Delta T'$ between the heat exchangers remains fixed. This is consistent with the increase in the Nusselt number defined by Eq. (1).

[35] A. A. Koronovsky and A. E. Khramov, *Continuous Wavelet Analysis and Its Applications* (Fizmatlit, Moscow, 2003) (in Russian).

[36] Wolfram Research, Inc., 100 Trade Center Drive, Champaign, IL 61820-7237, USA. WOLFRAM MATHEMATICA 9, 2012.

[37] J. Pantaloni, P. Ceresier, R. Bailleux, and C. Gerbaud, Convection de Bénard-Marangoni; un pendule foucault? J. Phys. (Paris) Lett. **42**, L147 (1981).

[38] N. Rivier, R. Occelli, J. Pantaloni, and A. Lissowski, Structure of Bénard convection cells, phyllotaxis and crystallography in cylindrical symmetry, J. Phys. (Paris) **45**, 49 (1984).